Coincidence detection of convergent perforant path and mossy fibre inputs by CA3 interneurons

Eduardo Calixto[1], Emilio J. Galván[2], J. Patrick Card[2] and Germán Barrionuevo[2]

[1]*División de Investigaciones en Neurociencias, Instituto Nacional de Psiquiatría Ramón de la Fuente, México City, México*
[2]*Department of Neuroscience, University of Pittsburgh, Pittsburgh, PA, USA*

We performed whole-cell recordings from CA3 s. radiatum (R) and s. lacunosum-moleculare (L-M) interneurons in hippocampal slices to examine the temporal aspects of summation of converging perforant path (PP) and mossy fibre (MF) inputs. PP EPSPs were evoked from the s. lacunosum-moleculare in area CA1. MF EPSPs were evoked from the medial extent of the suprapyramidal blade of the dentate gyrus. Summation was strongly supralinear when examining PP EPSP with MF EPSP in a heterosynaptic pair at the 10 ms ISI, and linear to sublinear at longer ISIs. This pattern of nonlinearities suggests that R and L-M interneurons act as coincidence detectors for input from PP and MF. Summation at all ISIs was linear in voltage clamp mode demonstrating that nonlinearities were generated by postsynaptic voltage-dependent conductances. Supralinearity was not detected when the first EPSP in the pair was replaced by a simulated EPSP injected into the soma, suggesting that the conductances underlying the EPSP boosting were located in distal dendrites. Supralinearity was selectively eliminated with either Ni^{2+} (30 μM), mibefradil (10 μM) or nimodipine (15 μM), but was unaffected by QX-314. This pharmacological profile indicates that supralinearity is due to recruitment of dendritic T-type Ca^{2+}channels by the first subthreshold EPSP in the pair. Results with the hyperpolarization-activated (I_h) channel blocker ZD 7288 (50 μM) revealed that I_h restricted the time course of supralinearity for coincidently summed EPSPs, and promoted linear to sublinear summation for asynchronous EPSPs. We conclude that coincidence detection results from the counterbalanced activation of T-type Ca^{2+} channels and inactivation of I_h.

(Received 18 February 2008; accepted after revision 3 April 2008; first published online 3 April 2008)
Corresponding author G. Barrionuevo: Department of Neuroscience, A210 Langley Hall, University of Pittsburgh, Pittsburgh, PA, USA. Email: german@bs.pitt.edu

Damage to the hippocampal formation in humans is known to produce a deficit in the ability to form long-term episodic memories (Eichenbaum & Otto, 1992). Although the mechanisms by which the hippocampus supports memory formation are still unknown, theoretical and empirical studies provide evidence that the neural network in area CA3 is capable of generating pattern separated memory representations from overlapping neocortical inputs from the entorhinal cortex (EC) (McNaughton & Morris, 1987; Treves & Rolls, 1994; O'Reilly & McClelland, 1994; Leutgeb *et al.* 2007). Pattern separation may require the reconfiguration of coincidentally active CA3 pyramidal cell assemblies by the coactivation of the two converging excitatory inputs from the EC. One input is conveyed monosynaptically via the perforant path (PP), the axons of the stellate cells in the EC layer II. The other input is conveyed disynaptically via the mossy fibres (MF), the axons of dentate gyrus (DG) granule cells, which also are the targets of the same layer II cells of the EC (Tamamaki & Nojyo, 1993). CA3 pyramidal cells receive strong somatic and dendritic inhibitory input from feedforward GABAergic interneurons (Buzsáki, 1984; Lawrence & McBain, 2003), which are innervated by the concurrent excitatory drive from both EC projections. The recruitment of feed-forward inhibitory interneurons to promote a narrow time window for pyramidal cell firing (Pouille & Scanziani, 2001) also may serve as a means for the orthogonalization of the CA3 representations. This inhibitory influence on the fine tuning of the active CA3 pyramidal cell assemblies during pattern separation may depend, in part, on whether integration of the excitatory inputs on interneurons is linear or nonlinear.

The ability of interneurons to integrate synaptic inputs with temporal reliability and precision has been attributed to the increased number and faster kinetics of postsynaptic AMPA/kainate receptors (Geiger *et al.* 1997; Nusser *et al.*

E. Calixto and E. J Galván contributed equally to this work. This paper has online supplemental material.

 DOI: 10.1113/jphysiol.2008.152751

1998; Walker *et al.* 2002; Jonas *et al.* 2004). Previous studies have also shown that interneurons are endowed with active conductances in somatic and dendritic compartments, similar to those found in pyramidal cells (Martina *et al.* 2000; Goldberg *et al.* 2003; Kaiser *et al.* 2004; Rozsa *et al.* 2004). These conductances could shape subthreshold EPSPs (Fricker & Miles, 2000; Jonas *et al.* 2004), and permit rapid detection of converging excitatory inputs (Galarreta & Hestrin, 2001). Although there have been extensive characterizations of the morphology, physiology and plasticity of CA3 interneurons (for reviews see Freund & Buzsáki, 1996; McBain *et al.* 1999; McBain & Fisahn, 2001; Lawrence & McBain, 2003; Jonas *et al.* 2004), the rules governing synaptic integration of MF and PP inputs to these cells are not known. The purpose of the current study was to assess the properties and mechanisms of temporal integration in radiatum (R) and stratum lacunosum-moleculare (L-M) interneurons in area CA3 by taking advantage of the ability to stimulate independently convergent MF and PP inputs (Urban & Barrionuevo, 1998). The axons of R and L-M interneurons branch in the s. lacunosum-moleculare, s. radiatum and s. pyramidale, and provide feed-forward inhibition to pyramidal cells (Lacaille & Schwartzkroin, 1988*b*; Williams *et al.* 1994; Vida *et al.* 1998). We performed somatic whole-cell recordings to measure the arithmetic summation of a series of pair-wise interactions between subthreshold AMPA MF and PP EPSPs evoked from the medial extent of the suprapyramidal blade of the dentate gyrus (SDG) at interstimulus intervals (ISI) ranging from 10 to 100 ms. We found that the prevalent summation rule at the 10 ms ISI was supralinearity brought about by the counterbalanced activation of T-type Ca^{2+} and inactivation of h channels. We propose that PP EPSP and MF EPSP were generated from neighbouring synapses located in the s. lacunosum-moleculare of area CA3.

Methods

Slice preparation

Animal use was in accordance with the University Institutional Animal Care and Use Committee. Male Sprague–Dawley rats (22 ± 4 days old; Zivic Miller Company) were deeply anaesthetized (Nembutal, I.P., 5 mg per 100 g body weight) and perfused intracardially with a modified artificial cerebrospinal fluid (ACSF) in which sucrose has been substituted for sodium chloride (concentrations in mM): 230.0 sucrose, 1.9 KCl, 1.2 $Na_2PO_4.7H_2O$, 25.0 $NaHCO_3$, 10.0 glucose, 1.0 $CaCl_2$, 4.0 $MgCl_2$, at 4°C; pH 7.3 maintained with bubbled O_2 (95%)/CO_2 (5%) at room temperature. Following 1–2 min of perfusion, animals were decapitated, and the brains removed. Blocks of tissue containing the hippocampus were glued to the stage of a Leica VT1000S vibrating blade microtome and were cut in 350 μm-thick sections. Slices were maintained for at least 60 min in an incubation solution of the following composition (in mM): 125 NaCl, 2.0 KCl, 1.2 NaH_2PO_4, 25.0 $NaHCO_3$, 10.0 glucose, 1.0 $CaCl_2$ and 6.0 $MgCl_2$, pH 7.4 maintained with bubbled O_2 (95%)–CO_2 (5%) at room temperature. The slices were transferred to a submersion recording chamber and superfused at constant flow (2.5 ml min^{-1}) with the following solution (in mM): 125 NaCl, 3.0 KCl, 1.25 Na_2HPO_4, 25 $NaHCO_3$, 2.0 $CaCl_2$, 1.0 $MgCl_2$, 10 glucose, 0.01 bicuculine; 0.05 D-2-amino-5-phosphonopentanoic acid (D,L-AP5), pH 7.4. Bath perfusion temperature was maintained at 33 ± 1°C.

Whole-cell recordings were obtained from the soma of putative interneurons in stratum radiatum (R) and stratum lacunosum-moleculare (L-M) of area CA3b of the hippocampus. Cell bodies were localized 60–80 μm from the slice surface, and identified visually with infrared video microscopy and differential interference contrast optics. Patch pipettes with electrical resistances of 3–6 MΩ were pulled from borosilicate glass and filled with a solution containing (in mM): 120 potassium methylsulphate, 10 KCl, 10 Hepes, 0.5 EGTA, 4.5 Mg.ATP, 0.3 Na_2GTP, 14 phosphocreatine. Biocytin, 0.5% (Molecular Probes, Eugene, OR, USA) was routinely added to the pipette solution to allow subsequent morphological identification and reconstruction of the neurons. Current clamp recordings were obtained with a Cornerstone amplifier (Model: BVC-700A, Dagan Corp., Minneapolis, MN, USA); voltage clamp recording were obtained with an Axoclamp-1D amplified (Axon Instruments, Union City, CA, USA). Signals were low-pass filtered at 3–5 kHz, digitized at 10 or 20 kHz, and stored on disk for off-line analysis. Data acquisition and analysis were performed using LabView (National Instruments, Austin, TX, USA) customized programs.

Electrophysiological measurements of membrane properties

The membrane potential was measured after initial break-in of the cell membrane. After the cell's membrane potential was stabilized in current-clamp, a series of inward and outward current steps (500 ms duration; 5–20 pA increments; 3–5 sweeps each at 0.2 Hz) were injected via the whole-cell pipette to assess input resistance (R_i), action potential (AP) amplitude, action potential threshold and afterhyperpolarization (AHP) amplitude. R_i was calculated as the slope of linear fit between voltage and injected current. AP amplitude was measured from AP threshold to the peak. AP threshold was calculated using two measurements as follows (Henze *et al.* 2000). First, the AP peak was determined by the first derivative of the membrane potential. Second, the threshold of the AP was determined by looking back from the AP peak to the

point where the third derivative of the membrane potential changed from negative to positive value. AHP amplitude was measured from AP threshold to the hyperpolarization peak. Classification of the firing pattern was based on the adaptation ratio (AR) of the first to last interspike interval to quantify the degree of spike adaptation within a sweep (Porter *et al.* 2001). For this measure, we chose a sweep that was evoked by a depolarizing current step of 150 pA above the current threshold for the first spike for each cell. Cells were classified as adapting (AR = 2.1), weakly adapting (AR = 1.2–2.0), and non-adapting (AR = 1.1; Kröner *et al.* 2007).

Stimulation techniques

Extracellular stimulation was performed using bipolar stimulating electrodes made of nichrome wire, 62 μm in diameter. Stimulation consisted of single monopolar pulses (100–300 μA intensity; 50–100 μs duration) at 0.2 Hz. To activate PP and minimize the spurious activation of MF (Henze *et al.* 1997), the stimulation electrode was placed in the s. lacunosum-moleculare of area CA1 far from area CA3, and close to the hippocampal fissure. In addition, to reduce the probability of antidromic stimulation of CA3 pyramidal cells and of activation of CA3 collaterals we use low current intensities, which result in responses with amplitude less than 30% of the threshold amplitude required to fire the interneurons. In a previous study (Berzhanskaya *et al.* 1998), a current source density analysis showed a sink restricted only to an area between 50 and 150 μm from the hippocampal fissure. This large sink was accompanied by a current source in the s. radiatum and was followed a few milliseconds later by a current source in the CA3 cell body layer. Under these conditions, no evidence was seen for current sinks in either the str. radiatum, or the cell body layer (s. pyramidale), indicating that the stimulation site in the s. lacunosum-moleculare results in specific activation of PP synapses. In all of the experiments the MF pathway was activated by placing the stimulating electrode in the medial extent of the SDG (Fig. 1*A* and *B*).

Generation of simulated EPSPs

Simulated EPSPs (simEPSPs) were elicited by somatic current injections generated using customized programs written in LabView, as previously described (Urban & Barrionuevo, 1998). The current waveform had a time course of an α function:

$$I(t) = I_o(t/\alpha)e^{2\alpha t}.$$

The value of α was between 0.018 and 0.05 and the magnitude was in the range between 0.001 and 0.005. This kind of current waveform reproduced accurately the time course of somatic EPSPs evoked by synaptic stimulation (Fig. 5*A*).

Measurement of temporal summation

Temporal summation was assessed off-line as previously described (Urban & Barrionuevo, 1998). Subthreshold MF and PP AMPA EPSPs with similar amplitudes were evoked alone and also in pairs at interstimulus intervals (ISIs) from 10 to 100 ms in 10 ms increments at a rate of 0.2 Hz. The independence of the inputs was assessed by verifying the lack of heterosynaptic pair pulse facilitation (PPF) between MF and PP inputs in voltage clamp conditions (Fig. 1*D*). In each experiment, we assessed the effect of each input on the other by first having MF stimulation precede the PP stimulation and then reversing the order, which allowed for the assessment of the effect of prestimulation of each of the inputs on the other. At each ISI, 10 combined EPSPs evoked by the paired stimulation were averaged. The first EPSP waveform of the pair was digitally subtracted from the 'Combined EPSP' waveform. This 'Subtracted EPSP' represents the second EPSP evoked by the paired stimulation. We calculated temporal summation as the ratio of the peak amplitude of the subtracted EPSP to the peak amplitude of the EPSP elicited alone from the second ('Actual EPSP'). A summation ratio (SR) = 1 indicates linear summation (the amplitude of the second EPSP in the pair is identical to the amplitude of the same EPSP evoked singly, i.e. subtracted EPSP = actual EPSP). Under these conditions, the combined effect of the subthreshold responses on the postsynaptic cell is determined by the arithmetic sum of the individual responses. When the amplitude of the subtracted EPSP is larger (SR > 1) or smaller (SR < 1) than that of the actual EPSP, summation is supra- or sublinear, respectively. That is, the combined effect of the subthreshold responses either exceeds or is below the arithmetic sum of the individual responses, respectively. By calculating the contribution of the second EPSP to the combined EPSP, this method allows us to identify the specific influence of each pathway on the other. We feel that this is particularly important, given the anatomical and functional differences between the MF and PP inputs. In experiments in which a simEPSP preceded either the MF or PP EPSP, SR was calculated as described above. To test the pharmacological effects of the drugs on the SR, single, combined and substracted EPSPs were measured in the presence of the different drugs used ($NiCl_2$, mibefradil, nimodipine or ZD 7288) and statistically compared to baseline summation.

Statistical analysis

Group measures are expressed as means ± S.E.M. To determine the statistical significance of the deviation from linear summation, SR values at each ISI interval were compared to SR values measured at 100 ms ISI; at this ISI, summation was always linear and not significantly different from the arithmetic sum of the individual EPSPs

elicited alone. In experiments with Ni^{2+} and ZD 7288, we also assessed the statistical significance of differences between SR in control *versus* treated slices. Significance was assessed by Student's paired *t* test or repeated-measures ANOVA followed by Dunnett's test contrasts. In all cases differences were considered significant if $P \leq 0.05$.

Morphological reconstruction

Following recordings, slices were fixed in cold 4% paraformaldehyde for 72 h, transferred into an antifreeze solution (one-to-one mixture of glycerol and ethylene glycol in 0.1 M phosphate buffer), and stored at −80°C. Slices were then cut into 60 μm sections

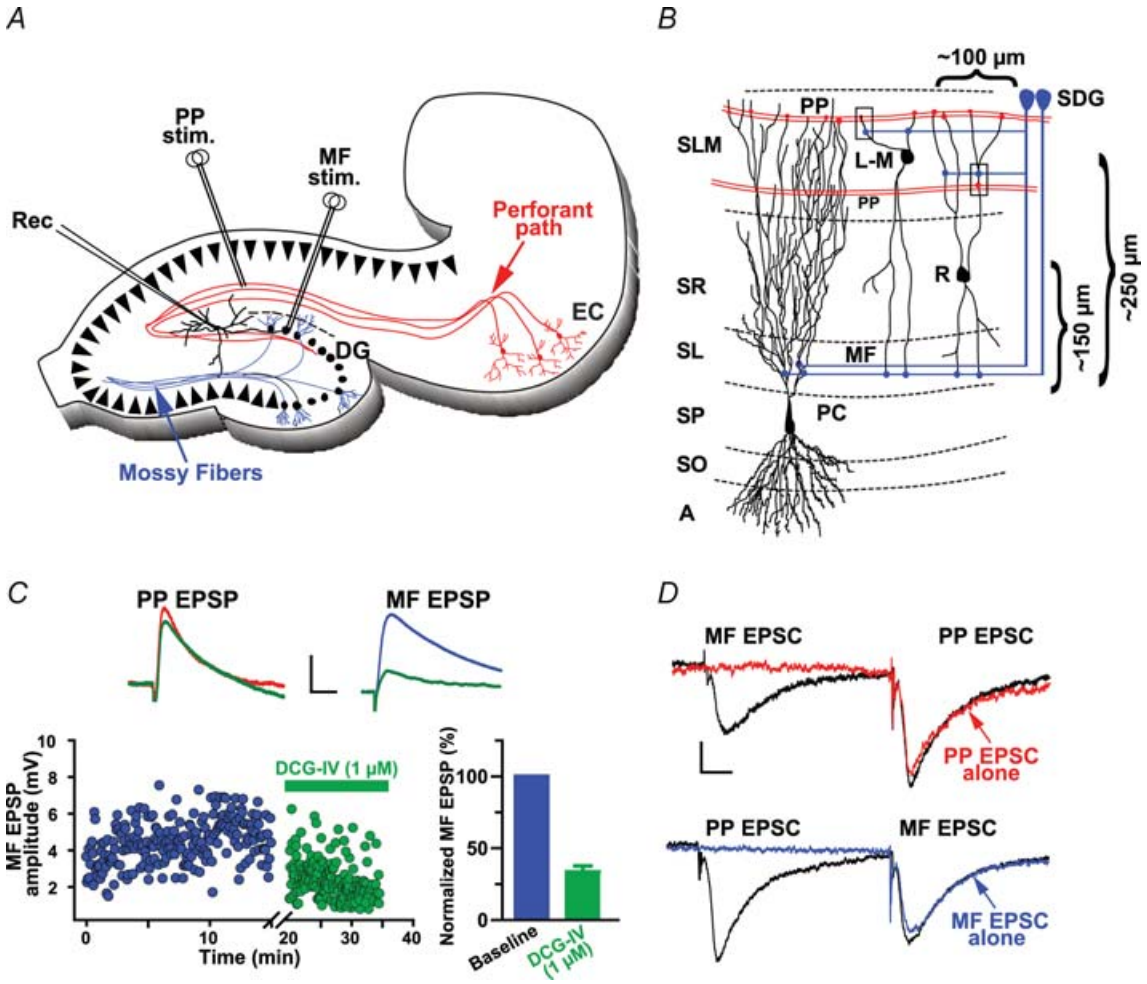

Figure 1. Synaptic responses in R and L-M interneurons
A, schematic representation of the hippocampal slice preparation depicting the position of the bipolar stimulation electrodes (Stim.) and the whole-cell recording pipette (Rec.). Perforant path fibres (red lines, PP) were activated from the s. lacunosum moleculare in area CA1. Mossy fibres (blue lines, MF) were activated from the suprapyramidal blade of dentate gyrus (SDG). *B*, schematic diagram of area CA3 showing the typical soma location of R and L-M interneurons relative to the boundary between s. pyramidale and s. lucidum. CA3 area receives convergent excitatory synaptic inputs from the entorhinal cortex and the dentate gyrus via the PP and the MF, respectively. PP courses through the s. lacunosum-moleculare making synaptic contacts on the distal dendrites of pyramidal cells and interneurons. Interneurons receive MF input via axon collaterals in the s. lacunosum moleculare near the hilus (SDG site), and from the MF axon trunks traveling in the s. lucidum (SL site). Recording were obtained from cells with soma at about 100 μm from the medial extent of the suprapyramidal blade of the dentate gyrus. Boxes indicate the possibility of neighbouring synapses from PP axons and the thin branches of MF axon collaterals. Abbreviations: A, alveus; SO, s.oriens; SP, s. pyramidale; SL, s. lucidum; SR, s. radiatum; SL-M, s. lacunosum-moleculare; MF, mossy fibres; PP, perforant path. *C*, averaged traces ($n = 10$) recorded from one L-M interneuron illustrating the selective reduction of MF EPSP by DCG-IV (1 μM). Scale: 2 mV, 25 ms. *D*, lack of interaction between MF and PP inputs as determined in heterosynaptic paired-pulse experiments (60 ms ISI) in voltage clamp. The amplitude of MF EPSC preceded by PP EPSC was 95.3 ± 9.9% of control (MF EPSC elicited alone). The amplitude of PP EPSC preceded by MF EPSC was 98 ± 14.7% of control (PP EPSC elicited alone). Average traces ($n = 10$). Scale bars 20 pA, 10 ms.

on a vibrating blade microtome, reacted with 1% H_2O_2 and placed in blocking serum with 0.5% Triton X-100 for 2 h at room temperature. Biocytin-labelled neurons were incubated with ABC-peroxidase and developed using the Ni-enhanced DAB chromogen. Interneurons were reconstructed using the Neurolucida tracing system (MicroBrightField, Inc., Williston, VT, USA) on an Axioplan 2 Zeiss microscope equipped with DIC, a 100× (NA = 1.4) planapochromatic lens and additional Optovar magnification of 1.6× (final optical magnification, 1600×; screen magnification, 7200×). For the reconstructions, all sections containing the cell were used.

Drugs

D,L-AP5 and DCG-IV were purchased from TOCRIS (Ellisville, MO, USA). All other drugs were from Sigma Chemical Co. (St Louis, MO, USA), and were prepared daily as concentrated stock solutions in water and diluted in external recording solution shortly before application.

Results

Anatomical and electrophysiological properties of R and L-M interneurons in area CA3

The somata of R and L-M interneurons included in this analysis were positioned $147 \pm 9.0\,\mu$m and $257.2 \pm 10.2\,\mu$m from the boundary between s. pyramidale and lucidum, respectively, and approximately $100\,\mu$m from the medial extent of the suprapyramidal blade of the dentate gyrus (Fig. 1*B*). Intrinsic membrane properties and morphological reconstructions were obtained from 23 R and 56 L-M interneurons. Representative examples of a reconstructed R and L-M interneurons are shown in Fig. 2*A* and *C*, respectively. Given the fact that the analysis focused on the potential sources of afferent input to R and L-M interneurons, we excluded the axons from the illustrations of reconstructed neurons in this report.

The majority of R (Fig. 2*A*) and L-M (Fig. 2*B*) interneurons were bipolar, with primary dendrites arising from the polar extremes of the somata. The morphology of each class of cell was consistent with that previously reported in the literature. Although the long axis of the dendritic arbors characteristic of each cell differed, the distal dendrites of each cell type were coextensive with the PP dorsally, and s. lucidum ventrally. In this regard, the distal branches of dorsal dendrites overlapped the PP at the dorsal blade of the dentate gyrus (compare insets *a* and *c* with *B* in Fig. 2) and apical dendrites at the ventral extent of the arbor invaded stratum lucidum and, in some cases, extended into stratum pyramidale. R and L-M interneurons had similar passive membrane properties (Table 1). Thirty-three per cent of the cells (8 R and 18 L-M interneurons) were adapting (AR = 3.2 ± 0.2). The majority of the cells (60%; $n = 10$ R and 13 L-M interneurons) had a weakly adapting firing pattern

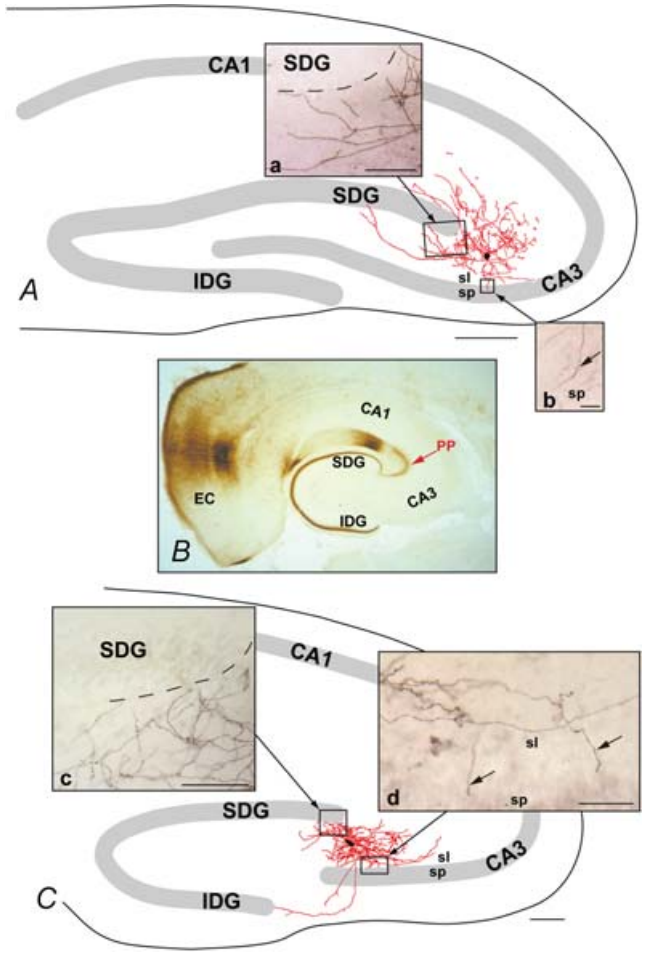

Figure 2. Computer reconstructions of the dendritic tree from biocytin-filled CA3 interneurons
Representative example of one L-M interneuron (*A*) and one R interneuron (*B*) filled with biocytin. The architecture of the dendritic arbors (mapped in red) typical of R and L-M interneurons included in this analysis are illustrated in *A* and *C*. *B* illustrates the trajectory of the perforant path (PP) axons revealed by the anterograde transport of biocytin from the entorhinal cortex (EC). The dendritic arbors were reconstructed from serial coronal section using Neurolucida software. Reconstructions were remapped onto templates that faithfully reproduced the location of s. pyramidale (sp.), the dentate gyrus and boundaries of the hippocampal formation in relation to the reconstructed cells. Both classes of interneurons gave rise to profusely branching dendritic arbors that bridged the area between stratum lucidum (sl) and the suprapyramidal blade of the dentate gyrus (SDG). Dorsally, the distal dendrites were near the medial extent of the SDG, and were coextensive with the PP axons (insets *a* and *c*). Ventrally, the distal dendrites of these arbors were present within s. lucidum, and coextensive with the MF axons (insets *b* and *d*, arrows). Marker bars = 500 μm for *A* and *C*, 100 μm for insets *a*, *c* and *d*, and 50 μm for insert b.

Table 1. Intrinsic Membrane Properties of R and L-M interneurons

Interneuron type	Membrane potential (mV)	Input resistance (MΩ)	Time constant (ms)	Action potential amplitude (mV)	Action potential duration (mV)	Action potential threshold (mV)	fAHP amplitude (mV)
R ($n = 23$)	-69 ± 0.5	190 ± 14	24.7 ± 0.91	79 ± 0.8	0.9 ± 0.09	-45 ± 0.8	12.01 ± 0.3
L-M ($n = 56$)	-68 ± 0.4	174 ± 10	21.2 ± 1.17	78 ± 1.1	1.0 ± 0.01	-46 ± 1.0	10.08 ± 0.4

Table 2. Properties of EPSPs in R and L-M interneurons ($V_m = -69$ mV)

Synaptic input	Onset latency (ms)	20–80% Rise-time (ms)	τ decay (ms)	Amplitude (mV)
MF EPSP ($n = 20$)	3.3 ± 0.7	2.0 ± 0.1	28.0 ± 3.5	3.2 ± 0.6
PP EPSP ($n = 20$)	3.2 ± 0.1	1.8 ± 0.1	27.0 ± 1.6	3.3 ± 1.2

(AR $= 1.7 \pm 0.75$). Only a small number of cells (7%; $n = 5$), all R interneurons, showed non adapting firing properties (AR $= 1.1 \pm 0.05$) (see online Supplemental material Fig. 1).

Synaptic excitation of R and L-M interneurons

In the presence of bicuculline and AP5, subthreshold MF and PP AMPA EPSPs (range 3–6 mV) were recorded at a resting potential of −69 mV (Table 2). Figure 1*C* shows typical PP and MF EPSPs evoked in one L-M interneuron. PP EPSPs were evoked from s. lacunosum-moleculare in area CA1 (Fig. 1*A*). MF EPSPs were evoked from the medial extent of the suprapyramidal blade of dentate gyrus (Fig. 1*A*). Application of the agonist for group-II metabotropic receptors (2*S*,2′*R*,3′*R*)-2-(2′3′-dicarboxycyclopropyl) glycine (DCG-IV; 1 μM) did not affect PP EPSP ($88.8 \pm 4.4\%$ of control; $P > 0.05$; $n = 7$; Fig. 1*C*) but significantly reduced MF EPSP ($36.9 \pm 1.8\%$ of control; $P < 0.001$; $n = 45$; Fig. 1*C*). Similar MF EPSP reduction with DCG-IV has been previously reported for the compound (Toth *et al.* 2000; Alle *et al.* 2001) and the unitary MF EPSC (Alle *et al.* 2001) in interneurons. We tested the MF EPSP sensitivity to DCG-IV data in each set of experiments but not in every recorded interneuron. In some experiments, MF axons in the s. lucidum were surgically transected by a micro-incision made under visual control after the slices were placed in the recording chamber (see online Supplemental material, Fig. 2*A* and *B*).

Supralinear summation of coincidently arriving subthreshold MF and PP inputs to R and L-M interneurons

In our previous work using the same experimental approach, we concluded that the sublinear summation of PP and MF EPSP in CA3 pyramidal cells results from the activation of transient potassium channels by the MF input (Urban & Barrionuevo, 1998). In the present work, we investigated whether temporal integration of PP EPSP and MF EPSP in CA3 interneurons also is shaped by voltage-dependent conductances. Therefore, we examined the temporal summation of subthreshold AMPA EPSPs from convergent MF and PP inputs in 16 interneurons (10 L-M and 6 R interneurons). As shown in Fig. 3*A* and *B*, each input was stimulated alone and also in conjunction with stimulation of the other input at ISIs ranging from 10 ms to 100 ms with interval increments of 10 ms. In each cell, MF stimulation preceded PP stimulation ('MF EPSP first'), and then the order was reversed ('PP EPSP first'). The distribution of SR values as a function of ISIs from 10 to 70 ms revealed a highly nonlinear pattern of synaptic summation with a progression from supra-linear to sublinear summation as the ISI was increased (Fig. 3). Given that the SRs for MF and PP responses were statistically equivalent across all ISIs, regardless of which input was stimulated first, the integration of these inputs does not depend on the temporal order of their activation. At the 10 ms ISI the magnitude of the second EPSP in the pair was significantly larger than the same EPSP evoked at 100 ms ISI when summation was linear. When MF EPSP preceded PP EPSP, SR was 1.36 ± 0.06 ($P < 0.001$); a comparable supralinearity was observed at this ISI when PP EPSP preceded MF EPSP (SR $= 1.41 \pm 0.08$; $P < 0.001$). The boosting to the second EPSP in the pair was no longer detected at the 20 ms ISI, and instead summation at this ISI was linear (SR $= 1.13 \pm 0.09$ with MF EPSP first; $P > 0.05$; SR $= 1.07 \pm 0.06$ with PP EPSP first; $P > 0.05$). The selective enhancement of summation for near synchronous EPSPs suggests that one main dendritic operation in R and L-M interneurons is coincidence detection (König *et al.* 1996). Indeed, for intervals between 30 and 60 ms, there was a gradual reduction in the magnitude of the second EPSP in the pair (Fig. 3*B*). The maximum sublinearity for both input permutations was at the 60 ms ISI (SR $= 0.47 \pm 0.09$, $P < 0.001$ with MF EPSP first; SR $= 0.51 \pm 0.10$, $P < 0.001$ with PP EPSP first). At ISIs longer than 60 ms, summation gradually became

linear, and at the 100-ISI the second EPSP in the pair was not significantly different from the same EPSP elicited singly (SR = 0.97 ± 0.02, MF EPSP first; SR = 0.93 ± 0.03, PP EPSP first; $P > 0.05$). Together these data demonstrate that small EPSPs (3–6 mV at the soma) from the first input are able to provide a substantial boost (~35%) to near synchronous EPSPs from the second input thereby potentially increasing the probability of postsynaptic firing in response to the conjoint input pattern.

Coincidence detection is mediated by postsynaptic conductances in distal dendrites

Whole cell recordings and confocal imaging studies have provided direct evidence indicating the presence of active conductances in interneuron dendrites and soma (Martina *et al.* 2000; Kaiser *et al.* 2001; Rozsa *et al.* 2004; Goldberg *et al.* 2003). Therefore, it is likely that subthreshold synaptic activation of a conductance with rapid activation kinetics could cause the supralinearity in temporal summation

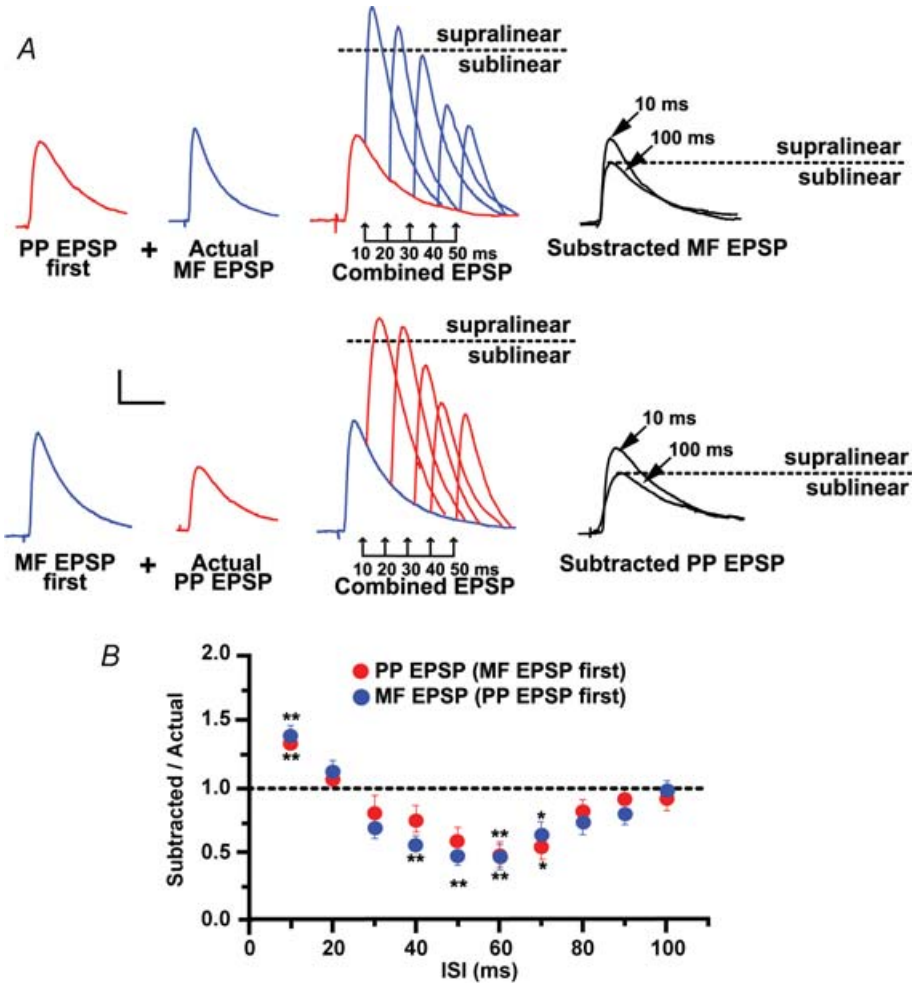

Figure 3. Coincidence detection of PP and MF inputs in area CA3 interneurons
A, representative experiment from one L-M interneuron depicting nonlinearities in the temporal summation of MF and PP EPSP. EPSPs are averaged traces ($n = 10$) evoked alone ('Actual'), and in pairs ('Combined EPSP') at the indicated ISIs. Right traces are averaged waveforms ($n = 15$) resulting from the digital subtraction ('Subtracted' EPSP) at the indicated ISIs. At 10 ms ISI, the subtracted EPSP is significantly larger than the corresponding EPSP evoked singly (supralinear summation) whereas at 60 ms ISI, the EPSP was significantly reduced (sublinear summation). Dotted line indicates the amplitude of the subtracted EPSP at the 100 ms ISI. *B*, population data ($n = 16$) showing a biphasic pattern of nonlinearities in EPSP summation. The ratio of the amplitude of subtracted EPSP to the amplitude of the second EPSP elicited alone was plotted as a function of ISIs ranging from 10 to 100 ms. Summation at 10 ms ISI was supralinear (summation ratio was increased by an average of 36% for PP EPSP first, and 41% for MF EPSP first). In contrast, summation at ISIs between 40 and 70 ms was sublinear (summation ratio was reduced by an average of 40% with PP EPSP or MF EPSP first). At the 100 ms ISI summation was linear (size of subtracted EPSP was not significantly different from actual EPSP). *Significant, $P < 0.05$. Error bars indicate S.E.M. Scale bars 2 mV, 20 ms.

between nearly coincident MF and PP EPSP. To test this hypothesis we performed similar experiments in somatic voltage clamp conditions ($V_h = -70$ mV). Low amplitude AMPA PP EPSC and MF EPSC (49 ± 6.1 pA and 46 ± 3.7 pA, respectively, $n = 9$; Fig. 4*A*) summed linearly at all ISIs regardless of the activation order. At the 10 ms ISI, the SR was 0.98 ± 0.06 when MF was stimulated first and 0.89 ± 0.04 when PP was stimulated first ($P > 0.05$; $n = 9$; Fig. 4*B*). At the 60 ms ISI, SR was 1.00 ± 0.07 with MF EPSC first and 0.92 ± 0.09 with PP EPSC first ($P > 0.05$ $n = 9$; Fig. 4*B*). These results indicate that the membrane properties of the R and L-M interneurons play a critical role in the detection of temporally coincident MF and PP inputs.

To gain insight into the relative contribution of somatic and dendritic conductances to the nonlinearities in summation, we substituted for the first EPSP in the pair a simulated EPSP (simEPSP) generated by somatically injecting synaptic-like currents via the whole cell pipette (see Methods). As shown in Fig. 5*A* and *B*, current injections were adjusted to elicit simEPSPs with comparable amplitude (3.1 ± 0.1 mV; $n = 10$) and time course (20–80% rise $= 2.1 \pm 0.2$ ms; $\tau_{decay} = 26.1 \pm 2.1$ ms; $n = 10$) to match the synaptically evoked EPSPs (Table 2). SR values at the 10 ms ISI calculated with simEPSP first ($n = 10$) were linear with MF or PP EPSP (0.94 ± 0.05 and 0.89 ± 0.06, respectively; $P > 0.05$; Fig. 5*B*). At longer ISIs, summation was sublinear and had a magnitude and time course comparable to that yielded with summed EPSPs at the same ISIs. Summation reached a sublinear peak at the 50 ms ISI (SR $= 0.63 \pm 0.06$; $P < 0.001$ with MF EPSP; SR $= 0.62 \pm 0.05$; $P < 0.001$ with PP EPSP) and gradually became linear at 100 ms ISI (0.99 ± 0.01; $P > 0.05$ with MF EPSP; SR $= 0.99 \pm 0.01$; $P > 0.05$ with PP EPSP; Fig. 5*B*). Previous studies have shown that the amplitude of artificial EPSPs generated at the pyramidal cell soma is reduced exponentially as it backpropagates to the dendritic tree (Stuart & Spruston, 1998; Williams & Stuart, 2000*b*). Furthermore, calcium transients in the interneuron dendrite are seldom evoked by backpropagating action potentials (Goldberg *et al.* 2004). Therefore, the lack of EPSP boosting when simEPSP was applied first suggests that coincidence detection is the result of voltage-dependent conductances in distal dendrites. We also conclude that sublinearity is produced by outward currents through voltage dependent channels localized in or near the soma.

The recruitment of supralinear boosting by the near synchronous activation of both inputs requires neighbouring synaptic positions on the dendritic tree (Cash & Yuste, 1999; Tamas *et al.* 2002; Polsky *et al.* 2004; Gasparini & Magee, 2006; Losonczy & Magee, 2006; Carter *et al.* 2007). As indicated by our reconstructions of

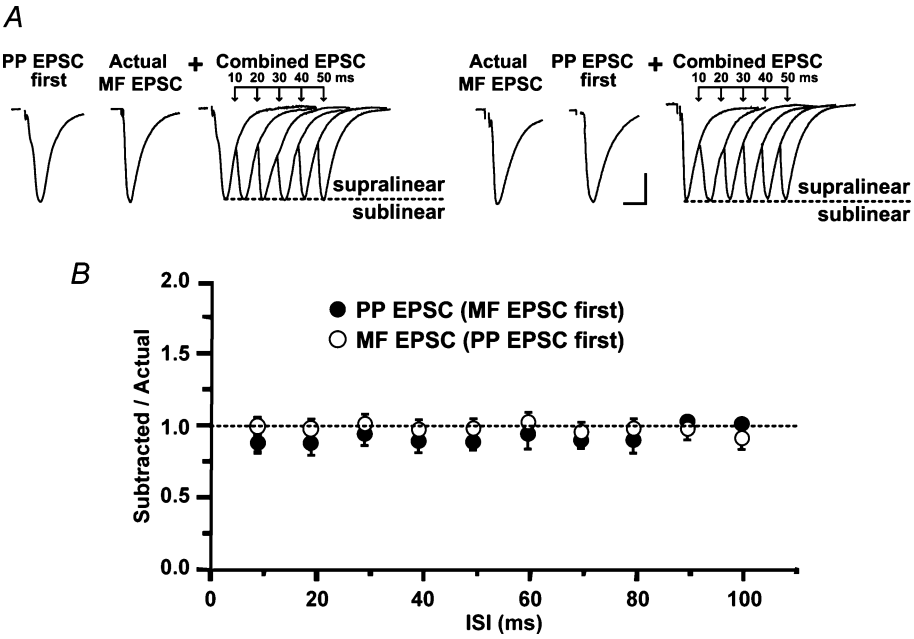

Figure 4. Coincidence detection is due to postsynaptic conductances
A, same experimental protocol described in Fig. 3 but performed in voltage clamp ($V_h = -70$ mV). Representative examples of an experiment depicting linear summation between MF and PP EPSCs (PP was stimulated first) in one L-M interneuron. Average PP and MF EPSC waveforms from 10 traces. Combined EPSC shows that the amplitude of the second EPSC is unchanged at the indicated ISI. Similar results were obtained when MF was stimulated first. *B*, group data showing that EPSC summation remained linear at all ISIs regardless of the order of input stimulation ($n = 9$). Error bars indicate S.E.M. Scale bars 20 pA, 20 ms.

the dendritic arbors, R and L-M interneurons have long branches extending into the s. lacunosum moleculare, in a region coextensive with the trajectory of PP fibres, which raises the possibility of synaptic activation of these neurons by PP synapses. Some of the same dendrites' branches in the s. lacunosum-moleculare extending near the SDG could receive input from the MF travelling to the s. lucidum or from MF collateral plexuses in the hilus of DG (Acsády *et al.* 1998; Claiborne *et al.* 1986; Fig. 1*B*). However, the anatomical reconstructions also indicate that R and L-M interneurons have dendrites that extend into s. lucidum and, occasionally, into the s. pyramidale (Fig. 2*A* and *C*), and could receive additional MF input via *en passant* synapses or filipodial extensions from MF boutons on CA3 pyramidal cells (Acsády *et al.* 1998). Synapses from MF axons in the s. lucidum and PP axons are placed far apart on dendritic trees ($< 200\ \mu$m) that emerge from parent dendrites arising from opposite poles of the interneuron soma. Given that temporally coincidental but spatially separated inputs sum linearly or sublinearly (Cash & Yuste, 1999; Tamas *et al.* 2002; Polsky *et al.* 2004; Gasparini & Magee, 2006; Losonczy & Magee, 2006; Carter *et al.* 2007), we were concerned that the concomitant activation of MF synapses in the s. lucidum could reduce the amount of supralinearity. We tested this possibility with a transection of area CA3 near the infrapyramidal blade of DG and across the s. radiatum, s. lucidum and s. pyramidale all the way through the s. oriens and alveus (Henze *et al.* 1997; see online Supplemental material, Fig. 2*A* and *B*). Transection of the MF trunks did not change significantly the supralinear summation between PP and MF (1.33 ± 0.09 with MF EPSP first; $n = 8$; $P > 0.05$; 1.32 ± 0.05 with PP EPSP first, $n = 8$; $P > 0.05$) (see online Supplemental material, Fig. 2*C* and *D*). Therefore, the supralinear summation we report is unlikely to be complicated by the activation of MF synapses in the s. lucidum.

Coincidence detection results from activation of the T-type calcium channel

Numerous observations support the contention that inward currents supplied by the low-threshold T-type Ca^{2+} (I_{CaT}) channels activated by subthreshold synaptic inputs underlie supralinear boosting (Markram & Sakmann, 1994; Magee & Johnston, 1995; Gillessen & Alzheimer, 1997; Randall & Tsien, 1997; Urban *et al.* 1998; Foehring *et al.* 2000). Early reports indicate the presence of low-threshold Ca^{2+} channels in the dendrites of L-M interneurons in area CA1 (Lacaille & Schwartzkroin, 1988*a*; Fraser & MacVicar, 1991). To examine whether the supralinear summation resulting from nearly coincident activation of MF and PP inputs is due inward currents

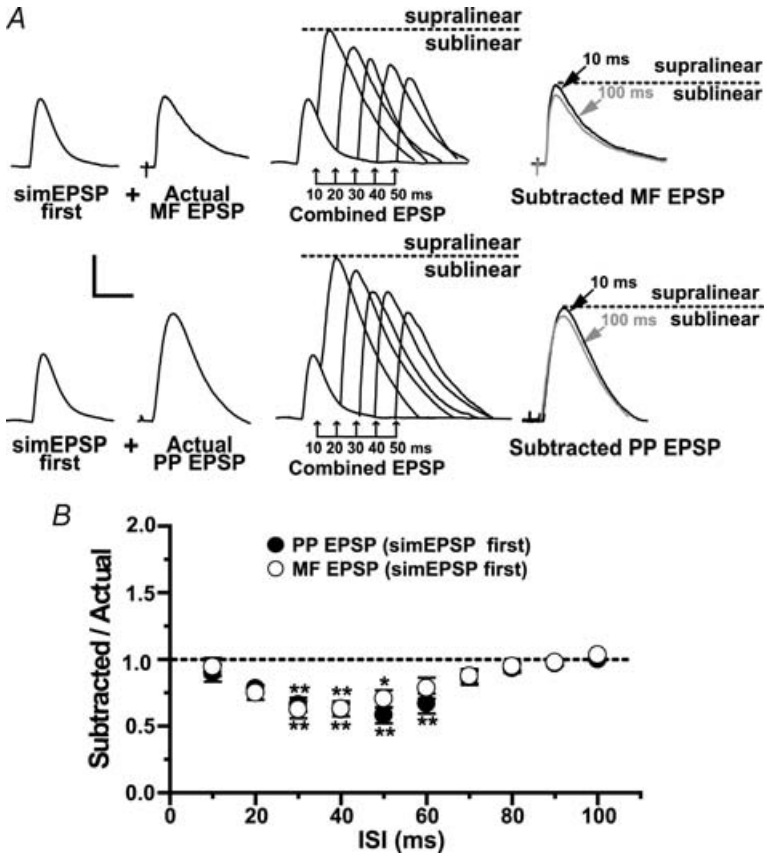

Figure 5. The postsynaptic conductances underlying coincidence detection are located in distal dendrites
A, typical example from a single experiment in one L-M interneuron in which the first EPSP in the pair was replaced by a simulated EPSP (simEPSP) generated by current injection of a synaptic-like waveform into the cell soma (see Methods). Same experimental protocol as described in Fig. 3. Traces are average voltage traces ($n = 15$) elicited singly. At 10 and 100 ms ISI, the subtracted EPSP had a magnitude similar to the EPSP evoked singly ('Actual'). Similar results were obtained with simEPSP preceding PP EPSPs. Dotted line indicates the amplitude of subtracted EPSP at the 100 ms ISI. *B*, in contrast to the case with EPSP summation, the mean distribution of summation ratios with simEPSP first shows no significant deviation from linearity at the 10 ms ISI ($n = 10$). At longer ISIs, summation with simEPSPs had a similar pattern of linearity (10–20 ms ISIs), and sublinearity (from 30 ms to 60 ms ISI for PP EPSP; from 30 to 50 ms ISI for MF EPSP) compared to summation between EPSPs shown in Fig. 3. *Significant, $P < 0.05$. Error bars indicate S.E.M. Scale bars 2 mV, 20 ms.

provided by I_{CaT}, we bath-applied low concentrations of $NiCl_2$ (30 μM). In contrast to previous studies in CA3 pyramidal cells (Urban *et al.* 1998; Breustedt *et al.* 2003; but see Gasparini *et al.* 2001), Ni^{2+} produced a small but significant reduction in EPSC amplitude with respect to control (EPSC = 77 ± 8.4%, $P < 0.05$, $n = 5$; PP EPSC = 71.7 ± 17%, $P < 0.05$, $n = 5$; data not shown) indicating that R-type Ca^{2+} channels contribute to baseline glutamatergic transmission at MF and PP synapses on R and L-M interneurons. Figure 6*B* show that at the 10 ms ISI, Ni^{2+} changed summation from supralinearity into a significant sublinearity with MF EPSP first (SR = 0.79 ± 0.05; $n = 10$; $P < 0.001$), and with PP EPSP first (SR = 0.88 ± 0.09; $n = 10$; $P < 0.001$). Ni^{2+} also affected summation at the 20 ms ISI. At this ISI, there was a significant sublinearity regardless of the activation order of the inputs (SR = 0.52 ± 0.06 with MF EPSP first, $P < 0.001$; SR = 0.68 ± 0.08 with PP EPSP first, $P < 0.001$; $n = 7$; Fig. 6*C*). In contrast, Ni^{2+} did not affect significantly the sublinearity at longer intervals (SR = 0.36 ± 0.02 with MF EPSP first and SR = 0.48 ± 0.27 with PP EPSP first; 50 ms ISI; $n = 7$; $P > 0.05$; Fig. 6*C*). In six cells, we also measured summation in the presence of mibefradil (10 μM), a preferential blocker of the T-type Ca^{2+} channel (Martin *et al.* 2000; Heady *et al.* 2001; Wolfart & Roeper, 2002). Unlike Ni^{2+}, Mibefradil did not affect significantly the EPSC amplitude (EPSC = 121.1 ± 21.6%; $P > 0.05$; PP EPSC = 109.8 ± 22.59%; $P > 0.05$; $n = 6$; data not shown) but produced a significant increase in input resistance (55.2 ± 4.3%; $P < 0.001$; Fig. 6*A*) most likely due to block of K^+ channels (Heady *et al.* 2001). Mibefradil also abolished the supralinearity at the 10 ms ISI with MF EPSP first (SR = 0.81 ± 0.06; $P < 0.001$; $n = 6$; Fig. 6), and PP EPSP first (SR = 0.72 ± 0.04, $P < 0.001$; Fig. 6*A* and *B*) but did not affect the sublinearity at longer intervals (SR = 0.75 ± 0.05 with MF EPSP first; SR = 0.60 ± 0.03 with PP EPSP first; $P > 0.02$). Because neither Ni^{2+} nor mibefradil is a specific T-channel blocker, these results indicate that coincidence detection also could be the result of R-type Ca^{2+} currents. However, nimodipine (15 μM),

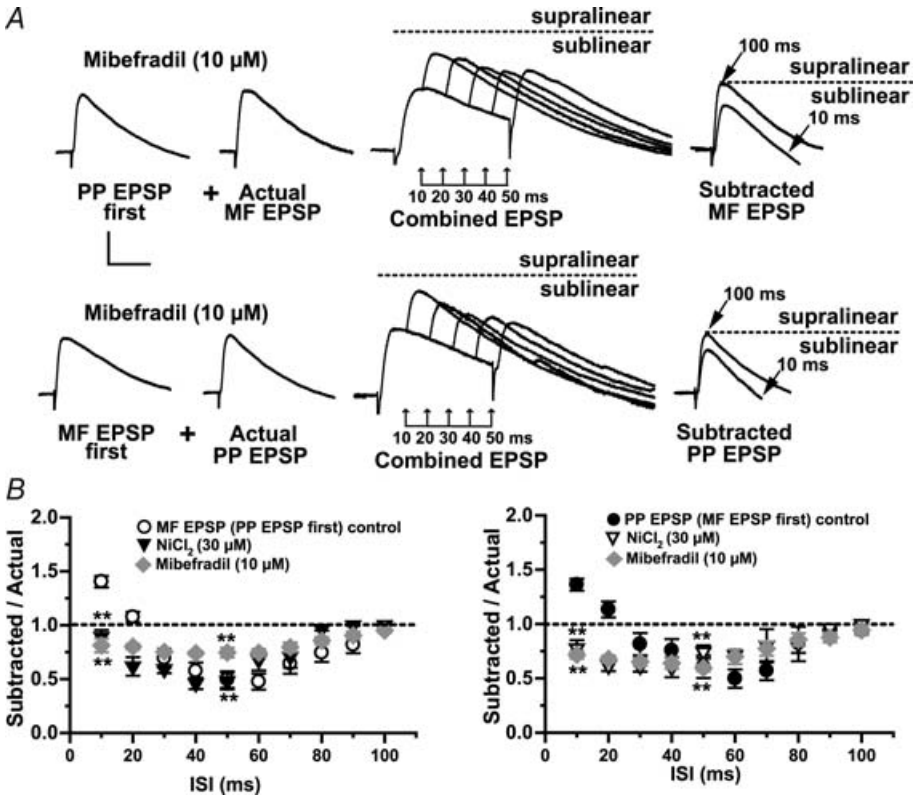

Figure 6. Coincidence detection relies on subthreshold activation of calcium currents
A, average traces ($n = 10$) are examples from a typical experiment in one L-M interneuron. Same experimental protocol as described in Fig. 3. At the 10 ms ISI, mibefradil resulted in significant reduction in the amplitude of subtracted EPSP (sublinear summation). In contrast, mibefradil did not affect the sublinearity typically present in control experiments at ISIs ranging from 50 to 70 ms. *B*, the mean group distribution of summation ratios reveals a similar block of supralinearity during bath applied Ni^{2+} ($n = 7$) and mibefradil ($n = 6$). Control data are the same as those shown in Fig. 3*B*. Dotted line indicates that the amplitude of the subtracted EPSP at the 100 ms ISI is identical to the amplitude of actual EPSP (linear summation). *Significant, $P < 0.05$. Scale bars 2 mV, 20 ms. Error bars indicate S.E.M.

which blocks T- but not the R-type Ca^{2+} channel (Randall & Tsien, 1997), abolished the supralinearity with MF EPSP first (SR = 0.72 ± 0.13; $P < 0.001$; $n = 8$; Fig. 7*A*), and PP EPSP first (SR = 0.87 ± 0.11; $P < 0.001$; $n = 8$; Fig. 7*A*. Like I_{CaT}, the persistent Na^+ current (I_{NaP}) is activated below the threshold for action potential firing (French *et al.* 1990), and has been shown to affect the amplitude and time course of single EPSPs in pyramidal cells (Stuart & Sakmann, 1995; Williams & Stuart, 1999), and fast spiking interneurons (Fricker & Miles, 2000; Galarreta & Hestrin, 2001). However, block of I_{CaT} switched summation from supra- to sublinearity (Fig. 6*B*), suggesting that Na^+ currents may not play a significant role in EPSP boosting. To address this issue directly, we assessed supralinearity in cells recorded with QX-314 (5 mM) in the pipette solution. QX-314 eliminated action potential firing evoked by intracellular injected outward currents, but had no effect on the supralinearity with EPSP first (SR = 1.34 ± 0.08 for MF; $P > 0.5$; $n = 7$) or PP EPSP first (SR = 1.40 ± 0.20 for; $P > 0.5$; $n = 7$). The pharmacological profile of the supralinearity based on the above results is summarized in Fig. 7*B* (control $n = 14$). In all, the data indicate that T-type Ca^{2+} current is the main contributor to the boosting of temporal coincident subthreshold MF and PP EPSP in R and L-M interneurons.

The time window for coincidence detection is determined by the hyperpolarization-activated cation (I_h) current

The magnitude of EPSP summation will depend on the balance between inward and outward currents. Several voltage-dependent ion channels can regulate neuronal excitability, including TEA- and 4-AP-sensitive K^+ channels, and h-channels. In contrast to the K^+ currents, the hyperpolarization-activated cation current, I_h,exerts its largest effects in the subthreshold range of membrane potentials and thus, it is well suited to influence the integration of excitatory synaptic inputs. In pyramidal cells, I_h plays an important role in influencing the integrative properties of dendrites by dampening dendritic excitability, normalizing temporal summation and accelerating the kinetics of the EPSP (Nicoll *et al.* 1993; Magee, 2000; Williams & Stuart, 2000*a*). A similar role for I_h has been observed in hippocampal interneurons (Maccaferri & McBain, 1996*b*; Svoboda & Lupica, 1998; Lupica *et al.* 2001; Aponte *et al.* 2006). To investigate the role of I_h in the temporal summation of MF and PP inputs, we bath applied the h-channel blocker 4-ethylphenylamino-1,2-dimethyl-6-methylaminopyrimidinium chloride (ZD 7288; 50 μM). In seven cells held at −69 mV, ZD 7288 produced significant membrane hyperpolarization (5.1 ± 1.3 mV; $P < 0.05$), and increased membrane resistance (75% ± 7.8) and the time constant (58% ± 17.2). Blockade of I_h also prolonged the decay time constant of MF EPSP (control = 27.8 ± 4.5 ms; pretreated with ZD 7288 = 49.3 ± 4.3 ms; $P < 0.001$), and PP EPSP (control = 25.8 ± 3.6 ms; pretreated with ZD 7288 = 54.9 ± 5.7; $P < 0.001$), but it did not change MF or PP EPSP amplitudes (89.6 ± 3.6% of MF EPSP and 94.6 ± 10.5% of PP EPSP). The absence of a ZD 7288 effect on EPSP amplitude may be attributed to the presence of two opposing actions of this drug that effectively cancel each other: block of I_h increases EPSP amplitude (Magee, 1998) whereas its inhibitory effect on AMPARs decreases EPSP amplitude (Chen, 2004). However, ZD 7288 had a pronounced effect on temporal

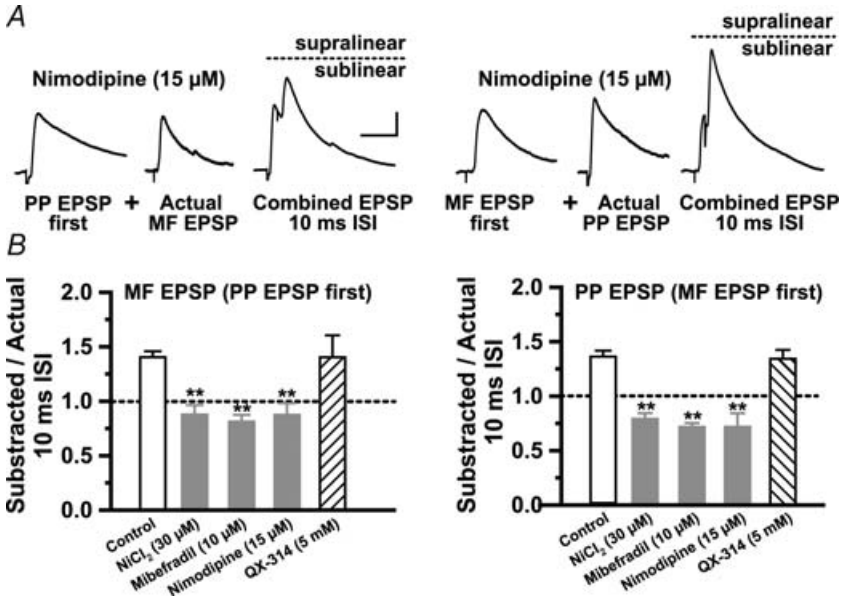

Figure 7. T-type calcium current is the main contributor to coincidence detection
A, traces are averaged waveforms ($n = 10$) from a representative experiment in one L-M interneuron showing the suppression of the supralinearity at the 10 ms ISI by nimodipine (15 μM). Dotted line in the combined EPSP indicates that the amplitude of the second EPSP at the 10 ms ISI is less than the amplitude of actual EPSP (sublinear summation). Scale bar 2 mV, 20 ms. *B*, the pharmacological profile of the supralinearity indicates that bath applications of Ni^{2+} (30 μM), mibefradil (10 μM) or nimodipine (15 μM) abolished the supralinearity and resulted in similar sublinear summation. Supralinearity was unaffected by QX-314 (5 mM).

summation. Figure 8 shows that supralinearity at the 10 ms ISI was enhanced (SR = 1.68 ± 0.17 with MF EPSP first, $P < 0.05$; SR = 1.59 ± 0.11 with PP EPSP first, $P < 0.05$; $n = 7$), and remained significantly increased up to the 30 ms ISI with MF EPSP first (1.38 ± 0.14; $P < 0.05$), and up to the 40 ms ISI with PP EPSP first (1.23 ± 0.13; $P < 0.05$).

The widening of the time window for EPSP boosting increased the cell's overall responsiveness to asynchronous inputs, thereby degrading coincidence detection. Furthermore, ZD 7288 changed summation from sublinear to linear between 50 and 70 ms ISIs with MF EPSP first (SR = 0.92 ± 0.12 at 50 ms ISI; $P > 0.05$; and SR = 0.85 ± 0.15 at 70 ms ISI with $P > 0.05$; Fig. 8*B*), and with PP EPSP first (SR = 1.08 ± 0.14 at 50 ms ISI, $P > 0.05$; and SR = 0.91 ± 0.09, $P > 0.05$ at 70 ms ISI; Fig. 8*B*). Consequently, I_h limited the temporal window for coincidence detection by restricting the time course of supralinearity and promoting linear to sublinear summation for asynchronous inputs. By controlling the temporal integration window, I_h is critically involved in determining the temporal precision of the interneuron response to inputs from PP and MF. Together our data suggest that R and L-M interneurons are able to detect millisecond shifts in the timing between temporally correlated subthreshold EPSPs through the counterbalanced activation of I_{CaT} and inactivation of I_h. A prediction from this hypothesis is that inputs will sum linearly at the 10 ms ISI if both conductances are blocked. In six cells, summation was measured in the presence of $NiCl_2$ (30 μM), and during the subsequent addition of ZD 7288 (50 μM) to the perfusion bath. As reported above, block of I_{CaT} by Ni^{2+} produced a significant sublinearity at the 10 ms ISI with MF EPSP first (SR = 0.79 ± 0.08; $P < 0.05$; $n = 4$; Fig. 9*A*) and with PP EPSP first (SR = 0.8 ± 0.16 C; $P < 0.05$; $n = 4$; Fig. 9*B*). In agreement with the prediction, summation became linear following the block of I_h (SR = 0.92 ± 0.12 for MF EPSP first; $n = 4$; SR = 0.93 ± 0.17 for PP EPSP first; $n = 4$; Fig. 9*A* and *B*).

Discussion

This study provides evidence that R and L-M interneurons in area CA3 possess voltage-dependent conductances which play a central role in shaping the temporal integration of converging EPSPs. Furthermore, the prominent supralinear boosting within a narrow time window suggests that these interneurons act as coincident detectors for subthreshold input from PP and MF. Previous studies in fast spiking (i.e. non-adapting) interneurons have ascribed coincidence detection of EPSPs

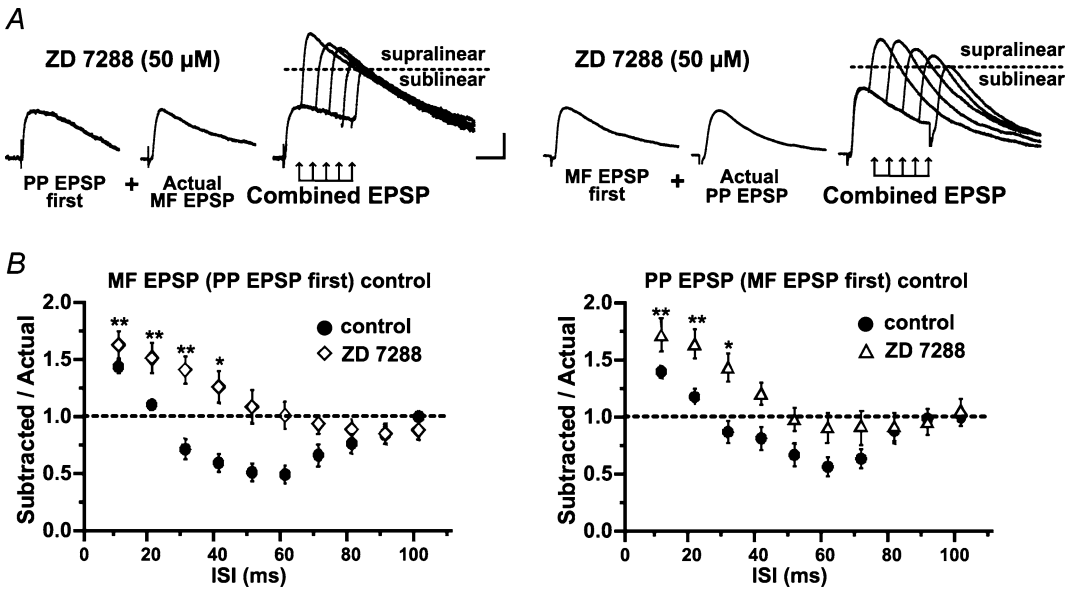

Figure 8. The temporal window for coincidence detection is determined by I_h
A shows representative traces ($n = 10$) from one experiment from one L-M interneuron treated with ZD 7288. Summation at the 40 ms ISI for MF EPSP first (left traces), and at the 40 ms ISI for PP EPSP first (right traces) are supralinear. Dotted line in the combined EPSP indicates the actual supralinearity at different ISIs. *B*, the mean group ($n = 7$) distribution of summation ratios during bath applied ZD 7288 (50 μM) revealed that the magnitude of supralinearity at the 10 ms ISI is significantly larger than control. Control data are the same as those shown in Fig. 3*B*. Supralinearity remained significant at the 30 ms ISI for MF EPSP first, and at the 40 ms ISI for PP EPSP first (for more details see Results). ZD 7288 also abolished the sublinearity present in control experiments at ISIs from 50 and 70 ms (Fig. 3); instead summation ratios at these intervals were linear. *Significant $P < 0.05$. Error bars indicate S.E.M. Scale 2 mV, 20 ms.

to increased number and faster kinetics of AMPA/kainate receptors (Geiger *et al.* 1997; Nusser *et al.* 1998; Walker *et al.* 2002; Jonas *et al.* 2004). The novel finding reported here is that adapting R and L-M interneurons are able to detect millisecond shifts in the timing between temporally correlated subthreshold EPSPs by the way of counterbalanced activation of voltage-dependent I_{CaT} and I_h channels. Specifically, we found that summation was supralinear for near coincident EPSPs (10 ms ISI). Non-coincident EPSPs summed linearly (20–30 ms ISI) to sublinearly (40–70 ms ISI). The prominent supralinear boosting within a narrow time span suggests that the integrative properties of R and L-M interneurons favour coincident detection for subthreshold EPSPs from PP and MF.

Characterization of R and L-M interneurons

The anatomical and electrophysiological properties of R and L-M interneurons reported here have been extensively characterized by previous work in areas CA1 and CA3 (Williams *et al.* 1994; Khazipov *et al.* 1995; Chitwood & Jaffe, 1998; Chitwood *et al.* 1999; Savić *et al.* 2001). Specifically, our interneurons correspond to the 'stellate cells' in area CA1 (Lacaille & Schwartzkroin, 1988*a*,*b*), and the interneurons at the s. radiatum–s. lacunosum-moleculare border (Kawaguchi & Hama, 1987; Kunkel *et al.* 1988; Williams *et al.* 1994; Perez *et al.* 2001). The spatial distribution of their dendritic trees in our cells also exhibit similarities with interneurons with the soma residing in the s. lacunosum-moleculare and radiatum described by others (Woodson *et al.* 1989; Gulyás *et al.* 1993; McBain & Dingledine, 1993; Arancio *et al.* 1994; Poncer *et al.* 1995; Maccaferri & McBain, 1996*a*,*b*; McMahon & Kauer, 1997) including the Schaffer collateral/commissural and perforant pathway-associated interneuron (Vida *et al.* 1998; Somogy & Klausberger, 2005). In area CA1, L-M interneurons are activated by PP input at a shorter latency and in a feed-forward manner, with respect to pyramidal cells indicating that these cells mediate feed-forward inhibition (Williams *et al.* 1994). The firing properties of CA3 R and L-M interneurons described here have adapting properties similar to the interneurons described by Chitwood & Jaffe, 1998). Interesting, L-M interneurons receive weak inhibitory input from other interneurons, which could potentially allow for a strong synaptic drive from their excitatory inputs (Williams *et al.* 1994).

Dependence of coincidence detection on I_{CaT} activation

Previous studies in pyramidal cells that reported coincidence detection using a similar paired stimulation protocol revealed the participation of regenerative Na^+ currents (Margulis & Tang, 1998), QX314 sensitive

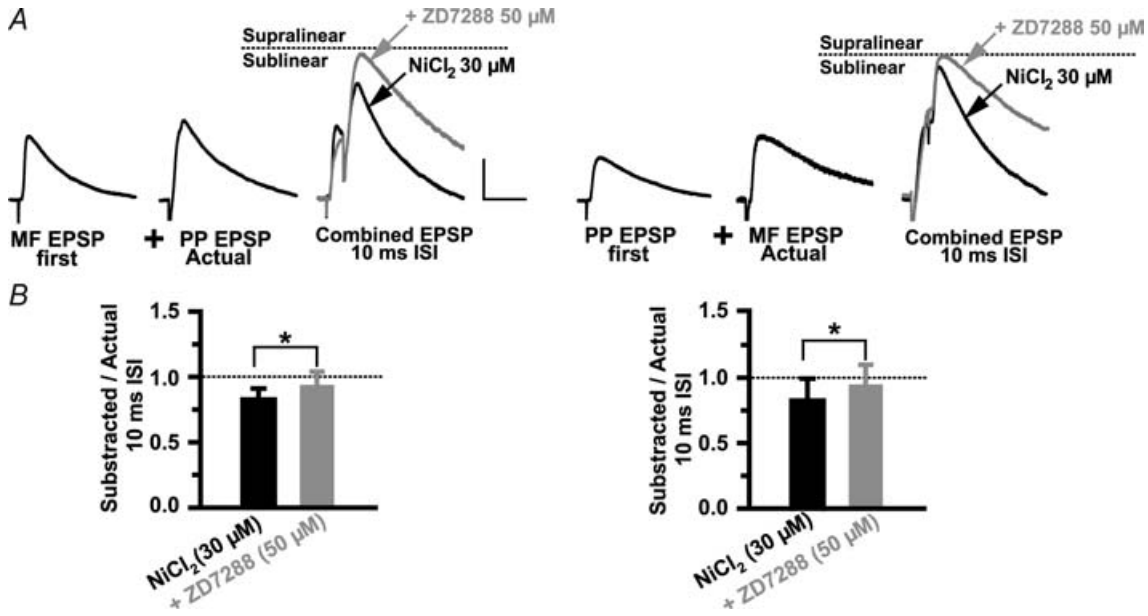

Figure 9. Coincident inputs sum linearly in the absence of both I_{CaT} and I_h
A, average traces ($n = 5$) from a representative experiment in one L-M interneuron showing the sublinear summation produced by Ni^{2+} and the reversal to linear summation by the subsequent application of ZD 7288 (grey trace). Scale 2 mV, 25 ms. *B*, the mean summation data (10 ms ISI; $n = 6$) show the switch from sublinearity to linearity by the addition of ZD 2788 to the bath perfusion containing Ni^{2+}. Dotted line indicates the amplitude of the second EPSP in the pair ('Actual' EPSP). *Significant, $P < 0.05$. Error bars indicate S.E.M.

conductances (Nettleton & Spain, 2000) or NMDAR activation (Polsky *et al.* 2004) in the boosting of the summed response. In fast spiking interneurons, the millisecond range in the temporal resolution of input synchronicity is attributable to the properties of post-synaptic receptors (Geiger *et al.* 1997; Nusser *et al.* 1998; Walker *et al.* 2002; Jonas *et al.* 2004), and the activation of voltage-dependent Na^+ channels (Galarreta & Hestrin, 2001). In the present study, supralinearity was unaffected by QX-314 but was sensitive to Ni^{2+} and mibefradil indicating an involvement of T- and/or R-type calcium currents. By contrast to R-type, T-type channels can be activated from only a few millivolts positive to −70 mV producing transient Ca^{2+} currents at potentials close to the cell's resting potential, typically −69 mV in our experiments. Furthermore, nimodipine, which does not affect the R-type channel (Randall & Tsien, 1997; Heady *et al.* 2001; Yasuda *et al.* 2003; Metz *et al.* 2005), abolished the supralinear boosting at a concentration of 15 μM. Based on a Hill slope of 1.61 and an IC_{50} value of 8.2 μM (Allen *et al.* 1993) we estimated that this concentration was sufficient to block 78% of I_{CaT}. Together, these pharmacological characteristics suggest that I_{CaT} is responsible for the majority of the inward currents for EPSP amplification in R and L-M interneurons. The density of T-type channels in pyramidal cells increases with distance from the soma (Magee & Johnston, 1995), and I_{CaT} is a prominent contributor to dendritic Ca^{2+} influx (Kavalali *et al.* 1997). These findings are consistent with the lack of supralinear summation with the somatic injections of simEPSP reported here. The dependence of I_{CaT} in coincidence detection also is in agreement with its role in the amplification of subthreshold EPSPs during propagation to the pyramidal cell soma (Sutor & Zieglagänsberger, 1987; Deisz *et al.* 1991; Markram & Sakmann, 1994; Magee & Johnston, 1995; Gillessen & Alzheimer, 1997; Andreasen & Lambert, 1998; Urban *et al.* 1998), and in neocortical interneurons (Goldberg *et al.* 2004). Interestingly, the time course of supralinearity described in the present work can be accounted for by the time-to-peak activation (∼10–30 ms) and time constant of inactivation (∼30–50 ms) of dendritic I_{CaT} (Magee & Johnston, 1995; Mouginot *et al.* 1997). A similar time dependence of the I_{CaT}-mediated enhancement of the second EPSP in a pair also has been observed in neocortical pyramidal cells (Deisz *et al.* 1991).

Dendritic compartmentalization of supralinear summation

The summation characteristics of convergent sub-threshold inputs are not solely determined by their relative timing, and the contribution of voltage-dependent conductances but, also by the dendritic localization and spatial separation between the synapses (Koch *et al.* 1983). In CA3 pyramidal cells, MF and PP inputs located far apart on the apical dendritic tree summate sublinearly at short ISIs with MF prestimulation (Urban & Barrionuevo, 1998). In contrast, synchronous inputs to neighbouring postsynaptic domains in thin branches of hippocampal and neocortical pyramidal neurons are able to summate supralinearly (Segev & London, 2000; Ariav *et al.* 2003; Polsky *et al.* 2004; Losonczy & Magee, 2006; Carter *et al.* 2007). For example, coincidental inputs to dendritic spines in the CA1 pyramidal cell show strong nonlinearity only if their spatial distribution is within 150 μm or less (Losonczy & Magee, 2006). However, this spatial requirement may be different for the spineless dendrite of the interneuron. Although we have no direct anatomical evidence for the localization of MF and PP synapses, our reconstructions of the interneuron dendritic tree suggest a similar anatomical arrangement formed by neighbouring synapses from PP axons and the thin branches of MF axon collaterals near the hilus. The observation that supralinear summation was unchanged after transection of the s. lucidum suggests that input to R and L-M interneurons elicited from the granule cells in the SDG site is largely mediated by axonal projections confined to dendrites near the hilus, in close proximity to PP synapses. However, as it is unavoidable for projection neurons *in vitro*, the negative finding may reflect truncation of MF by the slicing procedure, so the addition of the transection through the s. lucidum makes no additional impact on the circuitry of the slice.

In theory, pairs of coincident EPSPs from inputs in close spatial proximity would summate sublinearly due to shunting of the synaptic currents caused by the large increase in membrane conductance when both inputs are active. However, since the time course of the conductance that underlies AMPAR mediated synaptic transmission is several times faster than 10 ms (Geiger *et al.* 1997), it is unlikely that the two conductance changes overlapped significantly at this ISI. Indeed, summation was linear in the absence of I_{CaT} and I_h. However, synapses not only impose conductance changes but also inject currents onto highly localized dendritic regions. If PP and MF afferents make synapses close to each other, then their coincidental input mediated by current through AMPA receptors would produce a sufficient depolarization to recruit dendritic I_{CaT} thereby enhancing the second EPSP in the pair (Deisz *et al.* 1991). In particular, a high density distribution of I_{CaT} channels clustered near the synaptic sites, as shown in thalamocortical cells (Williams & Stuart, 2000*b*), could give rise to separate integrative compartments, each functioning as an independent supralinear computational unit (Segev & London, 2000; Ariav *et al.* 2003; Polsky *et al.* 2004; Losonczy & Magee, 2006). In this scheme, closely spaced supralinear compartments could give rise to reciprocal synaptic interactions that promote symmetrical boosting to near synchronous PP and MF

inputs. This interpretation is in agreement with the finding that the supralinear interaction between MF and PP afferents in R and L-M interneurons is symmetrical in time, i.e. prestimulation with either input amplifies the second EPSP in the pair. While the strong local depolarization evoked by the conjoint inputs might have evoked dendritic calcium spikes, EPSP waveforms at the 10 ms ISI were not inflected. However, smooth EPSPs in soma recordings could have resulted from dendritic filtering of distally located regenerative events.

The role of I_h in the temporal integration of MF and PP inputs

I_h has been shown to control the membrane properties of interneurons in the hippocampus (Maccaferri & McBain, 1996*a*; Svoboda & Lupica, 1998; Lupica *et al.* 2001; Aponte *et al.* 2006). In the present study, the hyperpolarizing shift observed following treatment with ZD 7288 points to a participation of I_h in the membrane conductance of R and L-M interneurons at potentials near rest. ZD 7288 also enhanced and prolonged the supralinearity, resulting in a considerable excitatory synaptic drive during both nearly coincident and temporally dispersed synaptic input. These data underscore the critical role of I_h in determining the temporal fidelity of coincidence detection, as demonstrated by previous experimental and computational studies (Magee, 1998; Jonas *et al.* 2004; Migliore *et al.* 2004; Yamada *et al.* 2005). From the data obtained with simEPSP first, we conclude that a significant proportion of I_h channels underlying the sublinearity are expressed at or near the interneuron soma. The block of I_{CaT} also reveals that integration in the region of temporal transition from supra- to sublinearity (~20 ms ISI) is the result of 'active linearization' (Cash & Yuste, 1999; Gasparini & Magee, 2006) by the dynamic counteracting activation of I_{CaT} and inactivation of I_h. For inputs arriving with progressively increasing asynchrony the mode of integration is sublinear and predominantly shaped by I_h inactivation. While blockade of I_h substantially reduced sublinearity over a range of ISIs, summation at ISIs up to 90 ms is sublinear in control conditions and in the presence of ZD 7288. Given these data, I_h cannot be expected to support this sublinearity (Magee, 1998). The D-type voltage gated potassium conductance (Storm, 1988; Metz *et al.* 2007) could be a candidate mediator of sublinear summation at long ISIs.

Functional implications

The time course of the supralinearity indicates that these cells could be selectively entrained by synaptic bursts elicited from the cells in the superficial layers of the EC firing at intervals (10–25 ms) time-locked to the intrinsically generated gamma oscillation (Charpak *et al.* 1995; Chrobak & Buzsáki, 1998). Because the supralinear interaction is symmetrical, i.e. it does not depend on the temporal order of cell firing between EC and dentate gyrus, R and L-M interneurons also are tuned to the phasic high frequency discharge (up to 100 Hz) from granule cells (Jung & McNaughton, 1993). Our data show that small EPSPs (3–6 mV at the soma) from the first input are able to provide a substantial boost ($< 35\%$) to near synchronous EPSPs from the second input thereby potentially increasing the probability of postsynaptic firing in response to the conjoint input. Thus, coincidence detection of correlated PP and MF input by R and L-M interneurons will likely synchronize their output targeting both the apical dendrite and soma of CA3 pyramidal cells in a feed-forward manner. The increased dendritic inhibition may gate the PP EPSP (Ang *et al.* 2005) by modulating the distal boosting by I_{CaT} (Urban *et al.* 1998); it also may control the induction of long-term synaptic plasticity in pyramidal cells by regulating the backpropagation of action potentials. On the other hand, the stronger feed-forward inhibition in the soma (Pouille & Scanziani, 2001) could constrain the timing of pyramidal cell discharge elicited by the converging input from the recurrent collaterals during the CA3-generated gamma oscillations. Thus, feed-forward inhibition may possibly sharpen the focus of the MF input to pyramidal cells when multiple cortical firing patterns are imposed to the CA3 network simultaneously, such as during pattern separation. Consistent with this line of reasoning is the observation that feed-forward inhibition is a key contributor to the sparsening of odour representations (Perez-Orive *et al.* 2002).

References

Acsády L, Kamondi A, Syk A, Freund T & Buzsaki G (1998). GABAergic cells are the major postsynaptic targets of mossy fibers in the rat hippocampus. *J Neurosci* **18**, 3386–3403.

Alle H, Jonas P & Geiger JRP (2001). PTP and LTP at a hippocampal mossy fiber-interneuron synapse. *Proc Natl Acad Sci U S A* **98**, 14708–14713.

Allen TG, Sim JA & Brown DA (1993). The whole-cell calcium current in acutely dissociated magnocellular cholinergic basal forebrain neurones of the rat. *J Physiol* **460**, 91–116.

Andreasen M & Lambert JD (1998). Factors determining the efficacy of distal excitatory synapses in rat hippocampal CA1 pyramidal neurones. *J Physiol* **507**, 441–462.

Ang CW, Carlson GC & Coulter DA (2005). Hippocampal CA1 circuitry dynamically gates direct cortical inputs preferentially at theta frequencies. *J Neurosci* **25**, 9567–9580.

Aponte Y, Cheng-Chang L, Reisinger E & Jonas P (2006). Hyperpolarization-activated cation channels in fast-spiking interneurons of rat hippocampus. *J Physiol* **574**, 229–243.

Arancio O, Korn H, Gulyás A, Freund T & Miles R (1994). Excitatory synaptic connections onto rat hippocampal inhibitory cells may involve a single transmitter release site. *J Physiol* **48**, 395–405.

Ariav G, Polsky A & Schiller J (2003). Submillisecond precision of the input-output transformation function mediated by fast sodium dendritic spikes in basal dendrites of CA1 pyramidal neurons. *J Neurosci* **23**, 7750–7758.

Berzhanskaya J, Urban NN & Barrionuevo G (1998). Pharmacological characterization of the monosynaptic perforant path input to CA3 pyramidal neurons. *J Neurophysiol* **79**, 2111–2118.

Breustedt J, Vogt KE, Miller RJ, Nicoll RA & Schmitz D (2003). α_{1E}-Containing Ca^{2+} channels are involved in synaptic plasticity. *Proc Natl Acad Sci U S A* **100**, 12450–12455.

Buzsáki G (1984). Feed-forward inhibition in the hippocampal formation. *Prog Neurobiol* **22**, 131–153.

Carter AG, Soler-Llavina GJ & Sabatini BL (2007). Timing and location of synaptic inputs determine modes of subthreshold integration in striatal medium spiny neurons. *J Neurosci* **22**, 8967–8977.

Cash S & Yuste R (1999). Linear summation of excitatory inputs by CA1 pyramidal neurons. *Neuron* **22**, 383–394.

Charpak S, Paré D & Llinás R (1995). The entorhinal cortex entrains fast CA1 hippocampal oscillations in the anaesthetized guinea-pig: role of the monosynaptic component of the perforant path. *Eur J Neurosci* **7**, 1548–1557.

Chen C (2004). ZD 7288 inhibits postsynaptic glutamate receptor-mediated responses at hippocampal perforant path-granule cell synapses. *Eur J Neurosci* **19**, 643–649.

Chitwood RA, Hubbard A & Jaffe DB (1999). Passive electrotonic properties of rat hippocampal CA3 interneurones. *J Physiol* **51**, 743–756.

Chitwood RA & Jaffe DB (1998). Calcium-dependent spike-frequency accommodation in hippocampal CA3 nonpyramidal neurons. *J Neurophysiol* **80**, 983–988.

Chrobak JJ & Buzsáki G (1998). Gamma oscillations in the entorhinal cortex of the freely behaving rat. *J Neurosci* **18**, 388–398.

Claiborne BJ, Amaral DG & Cowan WM (1986). A light and electron microscopic analysis of the mossy fibers of the rat dentate gyrus. *J Comp Neurol* **246**, 435–458.

Deisz RA, Fortin G & Zielglgansberger W (1991). Voltage dependence of excitatory postsynaptic potentials of rat neocortical neurons. *J Neurophysiol* **65**, 371–382.

Eichenbaum H & Otto T (1992). The hippocampus – What does it do? *Behav Neural Biol* **57**, 2–36.

Foehring RC, Mermelstein PG, Wen-Jie S, Ulrich S & Surmeier DJ (2000). Unique properties of R-type calcium currents in neocortical and neostriatal neurons. *J Neurophysiol* **84**, 2225–2236.

Fraser DD & MacVicar BA (1991). Low-threshold transient calcium current in rat hippocampal lacunosum-moleculare interneurons, kinetics and modulation by neurotransmitters. *J Neurophysiol* **11**, 2812–2820.

French CR, Sah P, Buckett KJ & Gage PW (1990). A voltage-dependent persistent sodium current in mammalian hippocampal neurons. *J Gen Physiol* **95**, 1139–1157.

Freund TF & Buzsáki G (1996). Interneurons of the hippocampus. *Hippocampus* **6**, 347–470.

Fricker D & Miles R (2000). EPSP amplification and the precision of spike timing in hippocampal neurons. *Neuron* **28**, 559–569.

Galarreta M & Hestrin S (2001). Spike transmission and synchrony detection in networks of GABAergic interneurons. *Science* **292**, 2295–2299.

Gasparini S, Kasyanov AM, Pietrobon D, Voronin LL & Cherubini E (2001). Presynaptic R-type calcium channels contribute to fast excitatory synaptic transmission in the rat hippocampus. *J Neurosci* **21**, 8715–8721.

Gasparini S & Magee JC (2006). State-dependent dendritic computation in hippocampal CA1 pyramidal neurons. *J Neurosci* **26**, 2088–2100.

Geiger JR, Lubke J, Roth A, Frotscher M & Jonas P (1997). Submillisecond AMPA receptor-mediated signaling at a principal neuron-interneuron synapse. *Neuron* **18**, 1009–1023.

Gillessen T & Alzheimer C (1997). Amplification of EPSPs by low Ni^{2+}- and amiloride-sensitive Ca^{2+} channels in apical dendrites of rat CA1 pyramidal neurons. *J Neurophysiol* **77**, 1639–1643.

Goldberg JH, Lacefield CO & Yuste R (2004). Global dendritic calcium spikes in mouse layer 5 low threshold spiking interneurons, implications for control of pyramidal cell bursting. *J Physiol* **558**, 465–478.

Goldberg JH, Tamas G & Yuste R (2003). Ca^{2+} imaging of mouse neocortical interneuron dendrites: Ia-type K^{+} channels control action potential backpropagation. *J Physiol* **551**, 49–65.

Gulyás A, Miles R, Hajos N & Freund TF (1993). Precision and variability in postsynaptic target selection of inhibitory cells in the hippocampal CA3 region. *Eur J Neurosci* **5**, 1729–1751.

Heady TN, Gomora JC, Macdonald TL & Perez-Reyes E (2001). Molecular pharmacology of T-type Ca^{2+} channels. *Jpn J Pharmacol* **85**, 339–350.

Henze DA, Gonzalez-Burgos G, Urban NN, Lewis DA & Barrionuevo G (2000). Dopamine increases excitability of pyramidal neurons in primate prefrontal cortex. *J Neurophysiol* **84**, 2799–2809.

Henze DA, Urban NN & Barrionuevo G (1997). Origin of the apparent asynchronous activity of hippocampal mossy fibers. *J Neurophysiol* **78**, 24–30.

Jonas P, Bischofberger J, Fricker D & Miles R (2004). Interneuron Diversity series. Fast in, fast out – temporal and spatial signal processing in hippocampal interneurons. *Trends Neurosci* **27**, 30–40.

Jung MW & McNaughton BL (1993). Spatial selectivity of unit activity in the hippocampal granule layer. *Hippocampus* **3**, 165–182.

Kaiser KM, Lübke J, Zilberter Y & Sakmann B (2004). Postsynaptic calcium influx at single synaptic contacts between pyramidal neurons and bitufted interneurons in layer 2/3 of rat neocortex is enhanced by backpropagating action potentials. *J Neurosci* **24**, 1319–1329.

Kaiser KM, Zilberter Y & Sakmann B (2001). Back-propagating action potentials mediate calcium signaling in dendrites of bitufted interneurons in layer 2/3 of rat somatosensory cortex. *J Physiol* **535**, 17–31.

Kavalali ET, Zhuo M, Bito H & Tsien RW (1997). Dendritic Ca^{2+} channels characterized by recordings from isolated hippocampal dendritic segments. *Neuron* **18**, 651–663.

Kawaguchi Y & Hama K (1987). Two subtypes of non-pyramidal cells in rat hippocampal formation identified by intracellular recording and HRP injection. *Brain Res* **411**, 190–195.

Khazipov R, Congar P & Ben-Ari Y (1995). Hippocampal CA1 lacunosum moleculare interneurons: modulation of monosynaptic GABAergic IPSCs by presynaptic $GABA_B$ receptors. *J Neurophysiol* **74**, 2126–2137.

Koch C, Poggio T & Torre V (1983). Nonlinear interactions in a dendritic tree: localization, timing, and role in information processing. *Proc Natl Acad Sci U S A* **80**, 2799–2802.

König P, Andreas K, Singer E & Singer W (1996). Integrator or coincidence detector? The role of the cortical neuron revisited. *Trends Neurosci* **19**, 130–137.

Kröner S, Krimer LS, Lewis D & Barrionuevo G (2007). Dopamine increases inhibition in the monkey dorsolateral prefrontal cortex through cell type-specific modulation of local circuit neurons. *Cereb Cortex* **17**, 1020–1032.

Kunkel DD, Lacaille JC & Schwartzkroin PA (1988). Ultrastructure of stratum lacunosum-moleculare interneurons of hippocampal CA1 region. *Synapse* **2**, 382–394.

Lacaille JC & Schwartzkroin PA (1988*a*). Stratum lacunosum-moleculare interneurons of hippocampal CAl region. I. Intracellular response characteristics, synaptic responses, and morphology. *J Neurosci* **8**, 1400–1410.

Lacaille JC & Schwartzkroin PA (1988*b*). Stratum lacunosum-moleculare interneurons of hippocampal CAl region. II lntrasomatic and intradendritic recordings of local circuit of synaptic recordings. *J Neurosci* **8**, 1411–1424.

Lawrence JJ & McBain CJ (2003). Interneuron diversity series: Containing the detonation – feedforward inhibition in the CA3 hippocampus. *Trends Neurosci* **26**, 631–640.

Leutgeb JK, Leutgeb S, Moser MB & Moser EI (2007). Pattern separation in the dentate gyrus and CA3 of the hippocampus. *Science* **315**, 961–966.

Losonczy A & Magee J (2006). Integrative properties of radial oblique dendrites in hippocampal CA1 pyramidal neurons. *Neuron* **50**, 291–307.

Lupica CR, Bell JA, Hoffman AF & Watson PL (2001). Contribution of the hyperpolarization-activated current (I_h) to membrane potential and GABA release in hippocampal interneurons. *J Neurophysiol* **86**, 261–268.

Maccaferri G & McBain CJ (1996*a*). Long-term potentiation in distinct subtypes of hippocampal non-pyramidal neurons. *J Neurosci* **16**, 5334–5343.

Maccaferri G & McBain CJ (1996*b*). The hyperpolarization-activated current (I_h) and its contribution to pacemaker activity in rat CA1 hippocampal stratum oriens-alveus interneurons. *J Physiol* **497**, 119–130.

McBain CJ & Dingledine R (1993). Heterogeneity of synaptic glutamate receptors on CA3 st. radiatum interneurones of rat hippocampus. *J Physiol* **462**, 373–392.

McBain CJ & Fisahn A (2001). Interneurons unbound. *Nat Rev Neurosci* **2**, 11–23.

McBain CJ, Freund TF & Mody I (1999). Glutamatergic synapses onto hippocampal interneurons: precision timing without lasting plasticity. *Trends Neurosci* **22**, 228–235.

McMahon LL & Kauer JA (1997). Hippocampal interneurons express a novel form of synaptic plasticity. *J Neurosci* **18**, 295–305.

McNaughton BL & Morris RG (1987). Hippocampal synaptic enhancement and information storage within a distributed memory system. *Trends Neurosci* **10**, 408–415.

Magee JC (1998). Dendritic hyperpolarization-activated currents modify the integrative properties of hippocampal CA1 pyramidal neurons. *J Neurosci* **18**, 7613–7624.

Magee JC (2000). Dendritic integration of excitatory synaptic input. *Nat Rev Neurosci* **1**, 181–190.

Magee JC & Johnston D (1995). Synaptic activation of voltage-gated channels in the dendrites of hippocampal pyramidal neurons. *Science* **268**, 301–304.

Margulis M & Tang CM (1998). Temporal integration can readily switch between sublinear and supralinear summation. *J Neurophysiol* **79**, 2809–2813.

Markram H & Sakmann B (1994). Calcium transients in dendrites of neocortical neurons evoked by single subthreshold excitatory postsynaptic potentials via low-voltage-activated calcium channels. *Proc Natl Acad Sci U S A* **91**, 5207–5211.

Martin RL, Lee JH, Cribbs L, Perez-Reyes E & Hanck DA (2000). Mibefradil block of cloned T-type calcium channels. *J Pharmacol Exp Ther* **295**, 302–308.

Martina M, Vida I & Jonas P (2000). Distal initiation and active propagation of action potentials in interneuron dendrites. *Science* **287**, 295–300.

Metz AE, Jarsky T, Martina M & Spruston N (2005). R-type calcium channels contribute to afterdepolarization and bursting in hippocampal ca1 pyramidal neurons. *J Neurosci* **25**, 5763–5773.

Metz AE, Spruston N & Martina M (2007). Dendritic D-type potassium currents inhibit the spike afterdepolarization in rat hippocampal CA1 pyramidal neurons. *J Physiol* **581**, 175–187.

Migliore M, Messineo L & Ferrante M (2004). Dendritic I_h selectively blocks temporal summation of unsynchronized distal inputs in CA1 pyramidal neurons. *J Comput Neurosci* **16**, 5–13.

Mouginot D, Bossu JL & Gahwiler BH (1997). Low-threshold Ca^{2+} currents in dendritic recordings from purkinje cells in rat cerebellar slice cultures. *J Neurosci* **17**, 160–170.

Nettleton JS & Spain WJ (2000). Linear to supralinear summation of AMPA-mediated EPSPs in neocortical pyramidal neurons. *J Neurophysiol* **83**, 3310–3322.

Nicoll A, Larkman A & Blakemore C (1993). Modulation of EPSP shape and efficacy by intrinsic membrane conductances in rat neocortical pyramidal neurons in vitro. *J Physiol* **468**, 693–710.

Nusser Z, Lujan R, Laube G, Roberts DB, Molnar E & Somogyi P (1998). Cell type and pathway dependence of synaptic AMPA receptor number and variability in the hippocampus. *Neuron* **21**, 545–559.

O'Reilly RC & McClelland JL (1994). Hippocampal conjunctive encoding, storage, and recall, avoiding a trade-off. *Hippocampus* **4**, 661–682.

Perez Y, Morin F & Lacaille JC (2001). A hebbian form of long-term potentiation dependent on mGluR1a in hippocampal inhibitory interneurons. *Proc Natl Acad Sci U S A* **98**, 9401–9406.

Perez-Orive J, Mazor O, Turner GC, Cassenaer S, Wilson RI & Laurent G (2002). Oscillations and sparsening of odor representations in the mushroom body. *Science* **297**, 359–365.

Polsky A, Mel BW & Schiller S (2004). Computational subunits in thin dendrites of pyramidal cells. *Nat Neurosci* **7**, 621–627.
Poncer JC, Shinozaki H & Miles R (1995). Dual modulation of synaptic inhibition by distinct metabotropic glutamate receptors in the rat hippocampus. *J Physiol* **485**, 121–134.
Porter JT, Johnson CK & Agmon A (2001). Diverse types of interneurons generate thalamus-evoked feedforward inhibition in the mouse barrel cortex. *J Neurosci* **21**, 2699–2710.
Pouille F & Scanziani M (2001). Enforcement of temporal fidelity in pyramidal cells by somatic feed-forward inhibition. *Science* **293**, 1159–1163.
Randall AD & Tsien RW (1997). Contrasting biophysical and pharmacological properties of T-type and R-type calcium channels. *Neuropharmacology* **36**, 879–893.
Rozsa B, Zelles T, Vizi ES & Lendvai B (2004). Distance-dependent scaling of calcium transients evoked by backpropagating spikes and synaptic activity in dendrites of hippocampal interneurons. *J Neurosci* **24**, 661–670.
Savić N, Pedarzani P & Sciancalepore M (2001). Medium afterhyperpolarization and firing pattern modulation in interneurons of stratum radiatum in the CA3 hippocampal region. *J Neurophysiol* **85**, 1986–1997.
Segev I & London M (2000). Untangling dendrites with quantitative models. *Science* **290**, 744–750.
Somogyi P & Klausberger T (2005). Defined types of cortical interneuron structure space and spike timing in the hippocampus. *J Physiol* **562**, 9–26.
Storm JF (1988). Temporal integration by a slowly inactivating K^+ current in hippocampal neurons. *Nature* **336**, 379–381.
Stuart G & Sakmann B (1995). Amplification of EPSPs by axosomatic sodium channels in neocortical pyramidal neurons. *Neuron* **15**, 1065–1076.
Stuart G & Spruston N (1998). Determinants of voltage attenuation in neocortical pyramidal neuron dendrites. *J Neurosci* **18**, 3501–3510.
Sutor B & Zieglagänsberger W (1987). A low-voltage activated, transient calcium current is responsible for the time-dependent depolarizing inward rectification of rat neocortical neurons in vitro. *Pflugers Arch* **410**, 102–111.
Svoboda KR & Lupica CR (1998). Opioid inhibition of hippocampal interneurons via modulation of potassium and hyperpolarization-activated cation (I_h) currents. *J Neurosci* **18**, 7084–7098.
Tamamaki N & Nojyo Y (1993). Projection of the entorhinal layer II neurons in the rat as revealed by intracellular pressure-injection of neurobiotin. *Hippocampus* **3**, 471–480.
Tamas G, Szabadics J & Somogyi P (2002). Cell type and subcellular position dependent summation of unitary postsynaptic potentials in neocortical neurons. *J Neurosci* **22**, 740–747.
Toth K, Suares G, Lawrence JJ, Philips-Tansey E & McBain CJ (2000). Differential mechanisms of transmission at three types of mossy fiber synapse. *J Neurosci* **20**, 8279–8289.
Treves A & Rolls ET (1994). Computational analysis of the role of the hippocampus in memory. *Hippocampus* **4**, 374–391.
Urban NN & Barrionuevo G (1998). Active summation of EPSPs in CA3 pyramidal neurons. *Proc Natl Acad Sci U S A* **95**, 11450–11455.
Urban NN, Henze DA & Barrionuevo G (1998). Amplification of perforant path EPSPs by sodium and LVA calcium channels in CA3 pyramidal cells. *J Neurophysiol* **80**, 1558–1591.
Vida I, Halasy K, Szinyei C, Somogyi P & Buhl EH (1998). Unitary IPSPs evoked by interneurons at the stratum radiatum-stratum lacunosum-moleculare border in the CA1 area of the rat hippocampus in vitro. *J Physiol* **506**, 755–773.
Walker HC, Lawrence JJ & McBain CJ (2002). Activation of kinetically distinct synaptic conductances on inhibitory interneurons by electrotonically overlapping afferents. *Neuron* **35**, 161–171.
Williams SR, Samulack DD, Beaulieu C & Lacaille JC (1994). Membrane properties and synaptic responses of interneurons located near the stratum lacunosum-moleculare/radiatum border of area CA1 in whole cell recordings from rat hippocampal slices. *J Neurophysiol* **71**, 2217–2235.
Williams SR & Stuart GJ (1999). Mechanisms and consequences of action potential burst firing in rat neocortical pyramidal neurons. *J Physiol* **521**, 467–482.
Williams SR & Stuart GJ (2000*a*). Site independence of EPSP time course is mediated by dendritic I_h in neocortical pyramidal neurons. *J Neurophysiol* **83**, 3177–3182.
Williams SR & Stuart GJ (2000*b*). Action potential backpropagation and somato-dendritic distribution of ion channels in thalamocortical neurons. *J Neurosci* **20**, 1307–1317.
Wolfart J & Roeper J (2002). Selective coupling of T-type calcium channels to SK potassium channels prevents intrinsic bursting in dopaminergic midbrain neurons. *J Neurosci* **22**, 3404–3413.
Woodson W, Nitecka L & Ben-Ari Y (1989). Organization of the GABAergic system in the rat hippocampal formation, a quantitative immunocytochemical study. *J Comp Neurol* **280**, 254–271.
Yamada R, Kuba H, Ishii TM & Ohmori H (2005). Hyperpolarization-activated cyclic nucleotide-gated cation channels regulate auditory coincidence detection in nucleus laminaris of the chick. *J Neurosci* **25**, 8867–8877.
Yasuda R, Sabatini BL & Svoboda K (2003). Plasticity of calcium channels in dendritic spines. *Nat Neurosci* **6**, 948–955).

Acknowledgements

We thank Ingeborg Kröener and John Cavaretta for their help with the interneuron reconstruction and technical support. This work was supported by NINDS grant NS24288

Supplemental material

Online supplemental material for this paper can be accessed at:
http://jp.physoc.org/cgi/content/full/jphysiol.2008.152751/DC1
and
http://www.blackwell-synergy.com/doi/suppl/10.1113/jphysiol.2008.152751